Elastic scattering and absorption of surface acoustic waves by a quantum dot

Andreas Knäbchen and Yehoshua B. Levinson
Weizmann Institute of Science, Department of Condensed Matter Physics, 76100 Rehovot, Israel

Ora Entin-Wohlman
School of Physics and Astronomy, Raymond and Beverly Sackler Faculty of Exact Sciences, Tel Aviv University, 69978 Tel Aviv, Israel
(Received 19 August 1996; revised manuscript received 25 October 1996)

The piezoelectric interaction of a surface acoustic wave (SAW) with a quantum dot is studied. Electron-electron interactions are accounted for by solving the screening problem in real space. The absorption and the scattering cross sections for SAW's as a function of the area of the dot, A, the sound wave vector, q, and the diffusion coefficient, D, of the electrons are calculated analytically in all cases where the quantities q^2A and $A\omega/D$ are larger or smaller than unity; ω is the SAW frequency. Numerical results cover the intermediate regimes. Based on the calculation of the weak localization corrections to the cross sections it is argued that scattering and absorption of sound as noninvasive probes may be advantageous in comparison to transport experiments for the investigation of small electronic systems, because for the former the phase coherence is enhanced as the system size shrinks. [S0163-1829(97)05808-6]

I. INTRODUCTION

During the last decade, several theoretical papers addressing the application of ultrasound for the investigation of quantum effects in disordered electronic systems have been published. Mainly, quantum corrections to the sound absorption in infinite systems have been studied.[1–5] The interaction of sound with electrons confined to a finite mesoscopic system has only been discussed with respect to the fluctuations of the ultrasound absorption,[6,7] emphasizing the idea that this is a noninvasive probe which can be used to investigate isolated metallic samples (no leads attached). The above calculations have essentially been done for the deformation potential interaction of bulk phonons with three-dimensional [3D] electron systems. To ensure an efficient coupling to the 3D phonon wave, the dimensionality of the electron system cannot be reduced, though this is necessary in order to enhance the weak localization (WL) effects. To overcome this restriction, we propose to consider the interaction of surface acoustic waves[8,9] (SAW's) with 2D electron systems.[10] This interaction is very strong in $GaAs/Al_xGa_{1-x}As$ heterostructures where it is caused by the piezoelectric field accompanying the SAW. Indeed, the SAW technique has been used successfully to investigate both the integer and the fractional quantum Hall regime.[11–15] Though the absorption of SAW's in these experiments is used to study extended electron systems, the SAW technique might be applied to mesoscopic systems as well. In this case, the noninvasive character of the measurement could prove advantageous. In a very recent experiment,[16] the direct acousto-electric current induced by a SAW through a *single* quantum point contact as small as 0.5 μm has been observed.

It is the main purpose of this paper to consider theoretically some of the effects associated with a noninvasive probing of mesoscopic 2D electron systems by SAW's. Specifically, we address the scattering and absorption of SAW's due to the electrons confined to an isolated quantum dot; see Fig. 1. The main quantities to be calculated are the elastic differential scattering cross section $\eta_{sc}(\boldsymbol{q}',\boldsymbol{q})$ and the absorption cross section $\eta_{abs}(\boldsymbol{q})$. (Though they have the dimension of a length in two dimensions, we use the familiar term cross section.) We compute the WL corrections to both η_{sc} and η_{abs}. Since the sample is isolated, the phase coherence is not reduced by leads which are necessarily attached to the dot in an electron transport measurement. This in turn affects the magnitude of the WL corrections and their dependence on the size of the dot. Though WL effects contribute only correction terms to the classical cross-sections, their dependence on weak magnetic fields and the phase coherence time (i.e., the temperature) can be used to detect them. Their particular dependence on the frequency is superimposed on that of the classical components of η_{sc} and η_{abs} and might therefore be difficult to resolve.

The screening of the electron-phonon coupling arises from the electrons confined to the dot and is not a negligible effect. We account for the screening in the linear response approximation, where the change of the electron density aris-

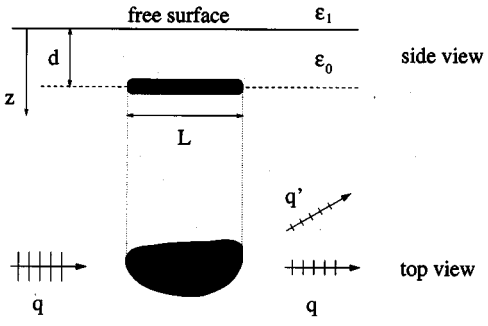

FIG. 1. Schematic drawing of the experiment. The quantum dot, shown in black, is of size L and is separated by a spacer layer of thickness d from the surface. The dielectric constants of the sample and the half-space above it are denoted by ϵ_0 and ϵ_1, respectively. The incoming and the transmitted waves have the wave vector $\boldsymbol{q}$, whereas $\boldsymbol{q}'$ is the wave vector of the scattered wave.

ing from the external perturbation is proportional to the magnitude of the perturbation. This approach is justified by the small SAW intensities used in experiments. Since we consider a system without translational invariance, the equations for the screened potential, the charge redistribution, etc. have to be formulated in real space. Consequently, screening cannot be taken into account by simply multiplying the unscreened potential by a dielectric function $\epsilon(\omega,\boldsymbol{q})$ but involves the inversion of the dielectric function (or matrix) $\epsilon(\boldsymbol{r},\boldsymbol{r}')$. To do this accurately, i.e., to account for the shape of the dot and the direction of the incoming SAW, we have performed numerical calculations. Analytically, one can exploit the fact that the screening is strong. In particular, for wavelengths $2\pi/q$ which are larger than the size L of the dot, a series expansion of ϵ^{-1} in terms of the small parameter a_B/L can be utilized, where a_B is the effective Bohr radius. This provides a rather complete qualitative understanding of the relations between the bare and the screened SAW potential and the charge redistribution in the dot.

In the calculation of the cross sections η_{sc} and η_{abs} we mainly focus on the cases where qL is of the order of or smaller than unity, and consider the diffusive limit, i.e., the size L of the dot is large compared to the elastic mean free path l. In addition, l has to be small compared to the wavelength $2\pi/q$ of the SAW, $ql \ll 1$. This relation guarantees $\omega\tau \ll 1$, because the velocity of sound, $s=\omega/q$, is much smaller than the Fermi velocity, $v_F=l/\tau$. From an experimental point of view, these conditions are satisfied in a dot of size $L \simeq 1$ μm, patterned in an electron gas with a low mobility ($\mu \simeq 10^4$ cm^2/Vs) corresponding to $l \simeq 100$ nm.

This paper is organized in the following way. In Sec. II, we summarize the main equations for the scattering and the absorption cross sections, the bare SAW potential arising from the piezoelectric coupling, and the dielectric function. The cross sections η_{sc} and η_{abs} and, within the linear screening approach, the dielectric function $\epsilon(\boldsymbol{r},\boldsymbol{r}')$ are essentially determined by the density-density correlator $\Pi_\omega(\boldsymbol{r},\boldsymbol{r}')$. This quantity is specified in Sec. III for the case of a diffusive system, where it comprises besides the classical term WL corrections. Based on these results, we discuss $\epsilon(\boldsymbol{r},\boldsymbol{r}')$ and its appropriate matrix representation in Sec. IV. An approximate inversion of ϵ is carried out analytically in the strong screening regime. This yields the screened potential in the dot in terms of the bare SAW field. Combining these results with the equations for $\Pi_\omega(\boldsymbol{r},\boldsymbol{r}')$, we evaluate the cross-sections in the limiting cases $qL \ll 1$ and $qL \gg 1$ in Sec. V. The weak localization corrections to η_{sc} and η_{abs} are related to the cooperon $\mathcal{C}_\omega(\boldsymbol{r},\boldsymbol{r})$. Its equation is solved in Sec. VI. Results of a numerical computation of the scattering and the absorption cross sections are presented in Sec. VII. A discussion is given in the last section.

II. BASIC EQUATIONS

The elastic scattering cross section, $\eta_{sc}d\varphi$, is the ratio of the sound intensity flux scattered into a ''solid'' angle $d\varphi$ around $\boldsymbol{q}'$ and the flux intensity I of the incoming surface wave with wave vector $\boldsymbol{q}$, $q=q'$. The absorption cross section determines the energy per unit time absorbed by the electrons in the dot from the acoustic wave field, $I\eta_{abs}$. Hence, it is directly associated with electron heating. The

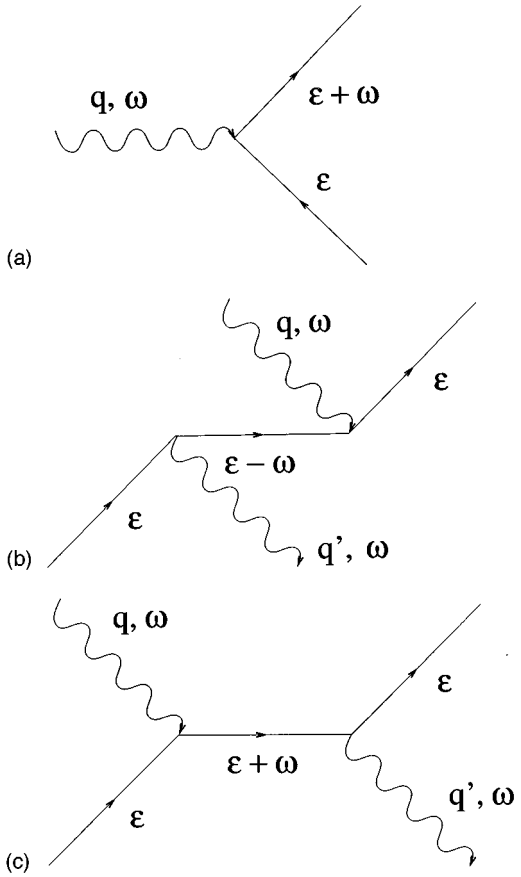

FIG. 2. Electron–surface-acoustic phonon interaction processes. The phonons are represented by wavy lines, and the electrons are depicted by straight lines. Diagram (a) shows the absorption of an incoming phonon (wave vector $\boldsymbol{q}$, energy ω). Diagrams (b) and (c) show scattering processes with two different intermediate states.

cross sections can be calculated from Fermi's golden rule. The amplitude for the absorption of a phonon results from a first-order process between the (phonon) states $|\boldsymbol{q}\rangle$ and $|0\rangle$, see Fig. 2; $\boldsymbol{q}$ is the 2D phonon wave vector. Scattering is a second-order process involving the two intermediate states $|\boldsymbol{q},\boldsymbol{q}'\rangle$ and $|0,0\rangle$ with two or no phonons. The absorption and (elastic) scattering cross sections have the form (a factor of 2 accounting for the spin degeneracy is included)

$$\eta_{abs}(\boldsymbol{q}) = -\frac{4\mathcal{L}^2}{s\hbar}\mathrm{Im}[\Pi_\omega(\boldsymbol{q},\boldsymbol{q})] \tag{1}$$

and

$$\eta_{sc}(\boldsymbol{q}',\boldsymbol{q}) = \frac{q\mathcal{L}^4}{\pi s^2\hbar^2}|\Pi_\omega(\boldsymbol{q}',\boldsymbol{q})|^2, \tag{2}$$

where s is the velocity of surface sound and

$$\Pi_\omega(\boldsymbol{q},\boldsymbol{q}') \equiv \int d^3\boldsymbol{R}\int d^3\boldsymbol{R}'\, V_{\boldsymbol{q}}^*(\boldsymbol{R})\Pi_\omega(\boldsymbol{R},\boldsymbol{R}')V_{\boldsymbol{q}'}(\boldsymbol{R}'). \tag{3}$$

Here, $\boldsymbol{R}$ is a 3D vector and $V_{\boldsymbol{q}}$ denotes the *screened* potential associated with one surface phonon with wave vector $\boldsymbol{q}$ in the normalization area $\mathcal{L}^2$ [which is canceled by a corresponding term originating from the SAW potential, see Eq.

(8) below]. The retarded density-density correlator $\Pi_\omega(\boldsymbol{R},\boldsymbol{R}')$ of the electrons in the dot is defined by

$$\Pi_\omega(\boldsymbol{R},\boldsymbol{R}')=-(i/\hbar)\int_0^\infty dt e^{i\omega t}\langle[\rho(\boldsymbol{R},t),\rho(\boldsymbol{R}',0)]\rangle, \quad (4)$$

where $\rho(\boldsymbol{R},t)$ is the electron density operator for one spin component and $\omega=qs$ is the SAW frequency. Below, we use the impurity-averaged density-density correlator in Eqs. (1) and (2).

Equation (3) can be simplified using the fact that the thickness of the 2D electron gas (2DEG) is much smaller than the penetration depth of the SAW into the interior of the sample. This allows one to neglect the finite extension of the 2DEG in the z direction, replacing $\rho(\boldsymbol{R},t)$ by $\delta(z-d)\rho(\boldsymbol{r},t)$, where d is the distance between the 2DEG and the surface of the sample and $\rho(\boldsymbol{r},t)$ is the areal density of 2D electrons. [We have $\boldsymbol{R}=(\boldsymbol{r},z)$ where $\boldsymbol{r}$ is a vector in the plane of the 2DEG and z is the coordinate perpendicular to it; see Fig. 1.] Substituting this replacement into Eq. (4) yields

$$\Pi_\omega(\boldsymbol{R},\boldsymbol{R}')=\delta(z-d)\,\delta(z'-d)\Pi_\omega(\boldsymbol{r},\boldsymbol{r}'), \quad (5)$$

where $\Pi_\omega(\boldsymbol{r},\boldsymbol{r}')$ is the 2D density-density correlator. Particle number conservation implies

$$\int d^2\boldsymbol{r}\Pi_\omega(\boldsymbol{r},\boldsymbol{r}')=\int d^2\boldsymbol{r}'\,\Pi_\omega(\boldsymbol{r},\boldsymbol{r}')=0. \quad (6)$$

Substituting Eq. (5) into Eq. (3), we obtain

$$\Pi_\omega(\boldsymbol{q},\boldsymbol{q}')\equiv\int d^2\boldsymbol{r}\int d^2\boldsymbol{r}'\,V^*_{\boldsymbol{q}}(\boldsymbol{r},z=d)\Pi_\omega(\boldsymbol{r},\boldsymbol{r}')\times V_{\boldsymbol{q}'}(\boldsymbol{r}',z'=d). \quad (7)$$

The integrations run over the area A of the dot.

The bare potential V^{ph} created by the SAW in the plane of the 2DEG can be represented in the form[17]

$$V^{ph}_{\boldsymbol{q}}(\boldsymbol{r},z=d)=\frac{1}{\mathcal{L}}\gamma_{\boldsymbol{q}}e^{i\boldsymbol{q}\boldsymbol{r}}. \quad (8)$$

For GaAs/Al_xGa_{1-x}As heterostructures and the range of wavelengths used in SAW experiments, the piezoelectric electron-phonon interaction is dominant. We may thus identify $\gamma_{\boldsymbol{q}}$ with the piezoelectric vertex $\gamma^{PA}_{\boldsymbol{q}}$, neglecting the deformation potential coupling. In addition, since qd is usually much smaller than unity, the dependence of $\gamma^{PA}_{\boldsymbol{q}}$ on d can be disregarded. (For $qd\sim1$, $\gamma_{\boldsymbol{q}}$ depends nonmonotonously on the parameter qd, see the discussion in Ref. 18.) Then we have

$$\gamma_{\boldsymbol{q}}=\gamma^{PA}_{\boldsymbol{q}}=(\hbar/\rho s a_{PA})^{1/2}\beta e\hat{q}_x\hat{q}_y=3.7\hat{q}_x\hat{q}_y10^{-10}\ \text{eV cm}, \quad (9)$$

where ρ is the mass density of the lattice, e is the electron charge, and a_{PA} represents a numerical factor that can be expressed in terms of the elastic constants of the lattice, cf. Ref. 17. Equation (9) is valid for a GaAs-type crystal with the SAW propagating along the (100) plane and electrically free[8] boundary conditions for the piezoelectric potential at the surface. In this case all (nonzero) piezoelectric moduli are equal to β. $\hat{q}_x$ (and, similarly, $\hat{q}_y$) is the component of $\hat{\boldsymbol{q}}$ in the direction of the lattice axis x on the surface. The numerical value [3.7] applies to GaAs/Al_xGa_{1-x}As heterostructures.

The potential V^{ph} associated with the SAW acts on the electrons in the dot and leads to their redistribution. This creates a potential V^{ch} that adds to V^{ph},

$$V=V^{ch}+V^{ph}, \quad (10)$$

where V determines the interaction of surface phonons with the electrons in the quantum dot; see Eq. (3). The calculation of V and the corresponding charge redistribution $\delta\rho(\boldsymbol{r})$ has to be done self-consistently. Bearing in mind that the quantum dot is embedded in a 3D semiconductor with dielectric constant ϵ_0, we have

$$\delta\rho(\boldsymbol{r})=2\int d^2\boldsymbol{r}'\Pi_\omega(\boldsymbol{r},\boldsymbol{r}')V(\boldsymbol{r}',z'=d), \quad (11)$$

$$\nabla^2V^{ch}(\boldsymbol{R})=-\frac{4\pi e^2}{\epsilon_0}\delta(z-d)\,\delta\rho(\boldsymbol{r}), \quad (12)$$

where the factor of 2 is due to spin degeneracy and the potentials and $\delta\rho(\boldsymbol{r})$ refer to the ω component in the corresponding Fourier expansions.

The solution of Poisson's equation (12) can be expressed in terms of the corresponding Green's function

$$\nabla^2G(\boldsymbol{R},\boldsymbol{R}')=-4\pi\delta(\boldsymbol{R}-\boldsymbol{R}'), \quad (13)$$

which has to satisfy the boundary conditions at the interface between the sample and the halfspace (dielectric constant ϵ_1) above it. Addressing the case where both $\boldsymbol{R}$ and $\boldsymbol{R}'$ lie in the plane of the dot ($z=z'=d$), we have

$$G(\boldsymbol{R},\boldsymbol{R}')=G(\boldsymbol{r}-\boldsymbol{r}')=\frac{1}{|\boldsymbol{r}-\boldsymbol{r}'|}+\frac{\epsilon_0-\epsilon_1}{\epsilon_0+\epsilon_1}\frac{1}{\sqrt{|\boldsymbol{r}-\boldsymbol{r}'|^2+(2d)^2}}. \quad (14)$$

The Green's function G can be combined with Eqs. (10)–(12) to relate the total potential directly to the SAW field

$$\int d^2\boldsymbol{r}'\,\epsilon(\boldsymbol{r},\boldsymbol{r}')V(\boldsymbol{r}',z'=d)=V^{ph}(\boldsymbol{r},z=d). \quad (15)$$

The kernel of this integral equation is the dielectric function

$$\epsilon(\boldsymbol{r},\boldsymbol{r}')=\delta(\boldsymbol{r}-\boldsymbol{r}')-2\frac{e^2}{\epsilon_0}\int d^2\boldsymbol{r}''G(\boldsymbol{r}-\boldsymbol{r}'')\Pi_\omega(\boldsymbol{r}'',\boldsymbol{r}'). \quad (16)$$

Using Eq. (6), one can see that $\int d^2\boldsymbol{r}'\,\epsilon(\boldsymbol{r},\boldsymbol{r}')=1$. This means that a potential that is spatially constant within the dot is not screened, cf. Eq. (15).

III. DENSITY-DENSITY CORRELATOR FOR A DIFFUSIVE SYSTEM

In the diffusive regime, the density-density correlator[19] has the form

$$\Pi_\omega(\boldsymbol{r},\boldsymbol{r}')=-\nu[\,\delta(\boldsymbol{r}-\boldsymbol{r}')+i\omega\mathcal{D}_\omega(\boldsymbol{r},\boldsymbol{r}')\,], \quad (17)$$

where $\mathcal{D}_\omega$ is the diffusion propagator and ν is the (2D) density of states for one spin projection. This result is valid for small frequencies $\omega\tau \ll 1$, small wave vectors $ql \ll 1$, and low temperatures $\omega, T \ll \epsilon_F$; ϵ_F is the Fermi energy. The wave number of the SAW, q, describes the spatial modulation of an external potential, the response to which can be expressed in terms of Π_ω, Eq. (17). Neglecting WL corrections, the diffusion propagator is given by[19]

$$[-i\omega - D\nabla^2]\mathcal{D}_\omega(\boldsymbol{r},\boldsymbol{r}') = \delta(\boldsymbol{r}-\boldsymbol{r}'), \quad \nabla_n \mathcal{D}_\omega|_b = 0, \tag{18}$$

where $D = l^2/2\tau$ is the 2D diffusion coefficient and ∇_n is the outer normal component of the gradient with respect to the boundary of the quantum dot. The boundary condition follows from the requirement that there is no flow of electrons through the boundary of the system. This is in contrast to a system coupled to leads, where $\mathcal{D}|_c = 0$ at the contacts.

The diffusion propagator, Eq. (18), can be expressed in terms of its (real) eigenfunctions ψ_m,

$$\mathcal{D}_\omega(\boldsymbol{r},\boldsymbol{r}') = \sum_{m=0}^{\infty} \frac{\psi_m(\boldsymbol{r})\psi_m(\boldsymbol{r}')}{-i\omega + D\lambda_m}, \tag{19}$$

defined by

$$[\nabla^2 + \lambda_m]\psi_m(\boldsymbol{r}) = 0, \quad \nabla_n \psi_m|_b = 0. \tag{20}$$

These form an orthonormal set, $\int d^2\boldsymbol{r}\psi_m\psi_n = \delta_{m,n}$. It is a peculiar feature of an isolated quantum dot that there exists a zeroth eigenfunction $\psi_0 = 1/\sqrt{A}$, A being the area of the dot. The corresponding eigenvalue $\lambda_0 = 0$ is well separated from the remaining sequence of eigenvalues $\lambda_m \sim A^{-1}$. The zeroth mode determines the behavior of the diffusion propagator in the case of a ''small'' dot, $A\omega/D \ll 1$. In this regime, the particle is able to diffuse through the whole system within one period of the external potential. Boundary effects are crucial and we obtain from Eq. (19) $\mathcal{D}_\omega(\boldsymbol{r},\boldsymbol{r}') \simeq (-i\omega A)^{-1}$. In the opposite, ''big-dot'' case, $A\omega/D \gg 1$, the particle diffuses only over a distance $\sqrt{D/\omega} \ll \sqrt{A}$ before the external potential is reversed. Thus, the diffusion process is bulk-like. Disregarding all boundary effects, Eq. (19) reduces in this case to the translational invariant form $\mathcal{D}_\omega(\boldsymbol{r}-\boldsymbol{r}')$, corresponding to an infinitely extended system. In the intermediate regime, $A\omega/D \simeq 1$, the diffusion propagator exhibits sample-specific properties.

Weak localization effects yield a correction, δD, to the classical diffusion coefficient D which basically describes the slowing down of the diffusion processes due to enhanced backscattering.[19,20] Generally, δD may depend on the frequency ω, the electron phase coherence time τ_ϕ, a weak magnetic field B, and other physical parameters. In addition, the WL correction acquires in a finite system a spatial dependence. To account for this, we replace[20] in Eq. (18)

$$D\nabla^2 \to \nabla[D + \delta D(\boldsymbol{r})]\nabla. \tag{21}$$

This replacement guarantees particle number conservation. Since we are only interested in first order corrections due to $\delta D(\boldsymbol{r})$, we write the diffusion propagator in the form $\mathcal{D}_\omega + \delta\mathcal{D}_\omega$. Substituting this ansatz in the modified Eq. (18) yields

$$\delta\mathcal{D}_\omega(\boldsymbol{r},\boldsymbol{r}') = \int d^2\boldsymbol{r}''\mathcal{D}_\omega(\boldsymbol{r},\boldsymbol{r}'')\{\nabla''\delta D(\boldsymbol{r}'')\nabla''\}\mathcal{D}_\omega(\boldsymbol{r}'',\boldsymbol{r}'). \tag{22}$$

Neglecting spin scattering, the WL correction can be expressed in terms of the cooperon[20,19] $\mathcal{C}$

$$\delta D(\boldsymbol{r}) = -\frac{D}{\pi\hbar\nu}\mathcal{C}_\omega(\boldsymbol{r},\boldsymbol{r}). \tag{23}$$

In real space, the cooperon obeys the equations[19]

$$\{-i\omega + \tau_\phi^{-1} + D[i\nabla + (2e/c\hbar)\boldsymbol{A}(\boldsymbol{r})]^2\}\mathcal{C}_\omega(\boldsymbol{r},\boldsymbol{r}') = \delta(\boldsymbol{r}-\boldsymbol{r}'),$$

$$[i\nabla_n + (2e/c\hbar)\boldsymbol{A}_n(\boldsymbol{r})]\mathcal{C}_\omega|_b = 0. \tag{24}$$

The effect of a (weak) magnetic field $\boldsymbol{B}$, oriented perpendicularly to the plane of the 2DEG, is described by the vector potential $\boldsymbol{A}(\boldsymbol{r})$. The boundary condition in Eq. (24) ensures that there is no flow of ''coherence'' ($\mathcal{C}$) through the boundary of an isolated system. The evaluation of the cooperon will be done in Sec. VI. For the rest of this and the next two sections it will be sufficient to bear in mind that $\delta D(\boldsymbol{r})$ is a well-defined quantity that can be calculated according to Eq. (23).

Let us now return to the density-density correlator. Substituting Eqs. (19) and (22) into Eq. (17) yields Π_ω in terms of the diffusion modes

$$\Pi_\omega(\boldsymbol{r},\boldsymbol{r}') = -\nu\sum_{m,n=1}^{\infty}\beta_{mn}\psi_m(\boldsymbol{r})\psi_n(\boldsymbol{r}'), \tag{25}$$

where

$$\beta_{mn} = \beta_m\delta_{m,n} + \delta\beta_{mn} \tag{26}$$

is decomposed into the classical term

$$\beta_m = \frac{D\lambda_m}{-i\omega + D\lambda_m} \tag{27}$$

and the WL contribution

$$\delta\beta_{mn} = \frac{-i\omega}{(-i\omega + D\lambda_m)(-i\omega + D\lambda_n)} \times \int d^2\boldsymbol{r}\delta D(\boldsymbol{r})\nabla\psi_m(\boldsymbol{r})\nabla\psi_n(\boldsymbol{r}). \tag{28}$$

The sums over modes in Eq. (25) start from $m,n = 1$ since $\beta_{m0} = \beta_{0m} = 0$ for $m = 0,1,\ldots$. This is a consequence of the structure of the diffusion propagator and holds true even for the case where $\delta D(\boldsymbol{r})$ is treated exactly (i.e., not only to first order). The restriction of the summations ensures that Π_ω fulfills Eqs. (6) since $\int d^2\boldsymbol{r}\psi_m = 0$ for $m \geqslant 1$.

IV. SCREENING

In order to apply Eq. (15) to the diffusive dot, we consider its representation in terms of the diffusion modes, Eq. (20). The matrix elements of the Green's function G, Eq. (14), can be written as

$$G_{mn} = \int d^2\boldsymbol{r}' \int d^2\boldsymbol{r}\psi_m(\boldsymbol{r})G(\boldsymbol{r}-\boldsymbol{r}')\psi_n(\boldsymbol{r}'). \tag{29}$$

For the potential V (and, similarly, for V^{ph}), we introduce the expansion

$$V(\boldsymbol{r},z=d)=\sum_{n=0}^{\infty} V_n\psi_n(\boldsymbol{r}), \quad V_n=\int d^2\boldsymbol{r}\psi_n(\boldsymbol{r})V(\boldsymbol{r},z=d). \tag{30}$$

Using these definitions, the complete set of equations which follows from Eq. (15) becomes

$$V_0^{ph}=V_0+2\frac{e^2\nu}{\epsilon_0}\sum_{n,l\geqslant 1} G_{0l}\beta_{ln}V_n, \tag{31}$$

$$V_m^{ph}=V_m+2\frac{e^2\nu}{\epsilon_0}\sum_{n,l\geqslant 1} G_{ml}\beta_{ln}V_n, \quad m\geqslant 1. \tag{32}$$

These equations have to be solved with respect to $\{V_n\}$. Not all of these quantities are coupled to each other. For example, as emphasized by Eqs. (31) and (32), the $\{V_n\}$, $n\geqslant 1$, form a closed system of equations. Its solution can be substituted into Eq. (31) determining the element V_0. This property of the screening equations results from the fact that, due to charge conservation, $\beta_{l0}=0$, cf. the discussion after Eq. (28).

The formal solution of Eq. (32) can be given in terms of an inverse dielectric matrix

$$V_m=\sum_{n\geqslant 1}(\epsilon^{-1})_{mn}V_n^{ph}. \tag{33}$$

The full numerical calculation of $(\epsilon^{-1})_{mn}$ is described in Sec. VII. Here, we present an analytical approach based on the following facts. First, the SAW potential is slowly varying on the scale of the dot, $qL\lesssim 1$. Consequently, only the first few elements V_n^{ph} are significantly different from zero, and we can concentrate on the matrix elements G_{mn}, β_{mn}, and $(\epsilon^{-1})_{mn}$ with indices m and n which are of order unity. Secondly, the screening in experimentally relevant samples is strong. To see this, we estimate the magnitude of the different terms in Eqs. (31) and (32). Using $\nu=m^*/2\pi\hbar^2$, the prefactor $2e^2\nu/\epsilon_0$ can be written in the form $1/\pi a_B$, where $a_B=\epsilon_0/e^2m^*$ is the effective Bohr radius of the lattice and m^* is the effective electron mass. Since $a_B=10.6$ nm for GaAs, the Bohr radius represents the smallest length scale in the system. The matrix element G_{mn} is of order $1/\sqrt{\lambda_m}\simeq L/m$ for $m\approx n$, $L\equiv\sqrt{A}$ being the size of the dot, and it decreases sharply for m or n much larger than unity and very different from each other. Hence, we have $(2e^2\nu/\epsilon_0)G_{mn}\simeq L/a_B$ for the relevant m and n of order unity. We therefore expect V_m to be of order $(a_B/L)V_m^{ph}\ll V_m^{ph}$.

An approximate inversion of Eq. (32) providing the leading terms in an expansion with respect to a_B/L can be accomplished by introducing the inverse matrix $(G^{-1})_{ml}$ to the reduced matrix G_{ml} with indices m and l equal to or larger than unity. Similarly, we define $(\beta^{-1})_{ml}$. Multiplying Eq. (32) with $\beta^{-1}G^{-1}$ yields for the inverse dielectric operator

$$(\epsilon^{-1})_{mn}=\frac{\pi a_B}{L}\sum_{l\geqslant 1}(\beta^{-1})_{ml}(\widetilde{G}^{-1})_{ln}+\mathcal{O}(a_B^2/L^2), \tag{34}$$

where $\widetilde{G}\equiv G/L$ is a dimensionless Green's function depending only on the shape of the dot.

Substituting Eqs. (34) and (33) into Eq. (31), we obtain for the $\boldsymbol{r}$-independent part of the total potential

$$V_0=V_0^{ph}-\sum_{n,l\geqslant 1} G_{0l}(G^{-1})_{ln}V_n^{ph}+\mathcal{O}(a_B/L). \tag{35}$$

This equation confirms explicitly the conclusion following from the general Eq. (16), namely that the spatially uniform part of an external potential, here V_0^{ph}, contributes unscreened to V_0. Moreover, since the product GG^{-1} is of order unity, it shows that also the spatially varying components V_n^{ph} contribute effectively unscreened to V_0. Combining Eqs. (34) and (35), we find for the total potential

$$V(\boldsymbol{r})\approx\frac{1}{\sqrt{A}}V_0+\frac{\pi a_B}{L}\sum_{m,n,l\geqslant 1}\psi_m(\boldsymbol{r})(\beta^{-1})_{mn}(\widetilde{G}^{-1})_{nl}V_l^{ph}. \tag{36}$$

Thus, in contrast to an open or an infinitely extended system, in the case of strong screening in an isolated dot one has a large but spatially constant background (the first term of order V^{ph}) in addition to the small, varying component (the second term) of the total potential. This behavior is based on particle conservation, for the charge on the dot can only be redistributed to some extent but cannot be increased or reduced via electrons flowing to or coming from the leads. But the absorption and scattering of phonons are associated only with the spatially varying component of the total potential which carries the factor $a_B/L\ll 1$. The screening of the SAW potential by the electrons in the quantum dot is thus an effect that reduces considerably the magnitude of the scattering and the absorption cross sections.

In concluding this section let us consider the charge redistribution $\delta\rho(\boldsymbol{r})$. Substituting Eqs. (25) and (36) into Eq. (11) yields

$$\begin{aligned}\delta\rho(\boldsymbol{r})&=-2\nu\delta(z-d)\sum_{m,n\geqslant 1}\psi_m(\boldsymbol{r})\beta_{mn}V_n\\&=-2\nu\delta(z-d)\frac{\pi a_B}{L}\sum_{m,n\geqslant 1}\psi_m(\boldsymbol{r})(\widetilde{G}^{-1})_{mn}V_n^{ph}\\&\quad+\mathcal{O}(a_B^2/L^2).\end{aligned} \tag{37}$$

That is, even in the strong screening case, where a_B is very small compared to other length scales, $\delta\rho(\boldsymbol{r})$ is determined by the distribution of the external potential within the whole dot. Indeed, the V_n^{ph} couple via nondiagonal elements of $\widetilde{G}^{-1}$ to other modes m. In this sense, screening in an isolated dot is strongly nonlocal.

V. SCATTERING AND ABSORPTION CROSS SECTIONS

In this section we study analytically the absorption and the scattering cross sections, Eqs. (1) and (2), in the limiting cases $qL\gg 1$ and $qL\ll 1$. The substantiation of these results by numerical calculations, addressing also the angular dependence of the cross sections, their sensitivity to the shape of the dot, etc., will be deferred until Sec. VII.

A. The case $qL \gg 1$

This regime resembles the case of an infinitely extended 2DEG. One may therefore use the usual $\boldsymbol{q}$ representation, leading to the relation $V(\boldsymbol{r}) = V^{ph}_{\boldsymbol{q}}(\boldsymbol{r})/\epsilon(\omega,\boldsymbol{q})$ between the total potential and the SAW field. The dielectric function

$$\epsilon(\omega,\boldsymbol{q}) = 1 + \frac{2\pi e^2}{\epsilon_0 q}\left[1 + \frac{1-\epsilon_1/\epsilon_0}{1+\epsilon_1/\epsilon_0}e^{-qd}\right]2\nu\beta(\omega,\boldsymbol{q}) \approx 1 + 2\frac{\beta(\omega,\boldsymbol{q})}{a_B q} \tag{38}$$

is derived from Eq. (16). Here,

$$\beta(\omega,\boldsymbol{q}) = \frac{(D+\delta D)q^2}{-i\omega + (D+\delta D)q^2} \tag{39}$$

is (except for the factor $-\nu$) the Fourier representation of the density-density correlator, Eq. (5), which replaces the expression β_{mn} [Eq. (25)] valid in the diffusion mode representation. To obtain Eq. (39), the WL correction $\delta D(\boldsymbol{r})$ has been replaced by the spatial average $\delta D = \text{const}$. Using $qd \ll 1$ and assuming $\epsilon_1 = 1 \ll \epsilon_0$, the dielectric function simplifies to the result given on the right-hand side of Eq. (38). The effective dielectric constant in the vicinity of the surface is then given by $(\epsilon_0+\epsilon_1)/2 \approx \epsilon_0/2$.

Substituting the bare SAW potential [Eq. (8)] and the dielectric function $\epsilon(\omega,\boldsymbol{q})$ [Eq. (38)] in Eq. (7) for the quantity $\Pi_\omega(\boldsymbol{q},\boldsymbol{q}')$, we obtain for the absorption cross section

$$\eta_{abs}(\boldsymbol{q})/A = \frac{4\nu}{s\hbar}|\gamma_{\boldsymbol{q}}|^2 \frac{\mathrm{Im}[\beta(\omega,\boldsymbol{q})]}{|\epsilon(\omega,\boldsymbol{q})|^2} \equiv \Gamma_{\boldsymbol{q}}, \tag{40}$$

where $\Gamma_{\boldsymbol{q}}$ is the attenuation coefficient[8] of a SAW in an infinite 2DEG. Neglecting WL corrections, the attenuation coefficient given in Eq. (40) coincides with the result following from the well-known treatment of sound absorption due to the piezoelectric interaction (see, e.g., Refs. 12 and 18). In the case of strong screening, Eq. (40) becomes

$$\Gamma_{\boldsymbol{q}} = \frac{\nu}{s\hbar}|\gamma_{\boldsymbol{q}}|^2 (a_B)^2 \frac{\omega}{D}\left(1 - \frac{\mathrm{Re}[\delta D]}{D}\right) = \frac{1}{2}K^2_{\mathrm{eff}} q \frac{\sigma_m}{\sigma}\left(1 - \frac{\mathrm{Re}[\delta\sigma]}{\sigma}\right), \tag{41}$$

where the right-hand side uses the ''standard'' notation, i.e., $\Gamma_{\boldsymbol{q}}$ is given in terms of the 2D conductivity σ, the conductivity $\sigma_m \equiv \epsilon_0 s/4\pi$, and the effective electromechanical coupling coefficient $K^2_{\mathrm{eff}} = |\gamma_{\boldsymbol{q}}|^2 \epsilon_0/2\pi s e^2\hbar$. Equation (41) shows that the WL corrections can be incorporated into the classical result by replacing D by $\mathrm{Re}[D+\delta D]$ or σ by $\mathrm{Re}[\sigma+\delta\sigma]$, where $\delta\sigma$ is the corresponding correction of the conductivity. Since the WL effects slow the diffusion processes down, $\mathrm{Re}[\delta D] \sim \mathrm{Re}[\delta\sigma] < 0$, they reduce the screening of the SAW field which in turn gives rise to an enhancement of the absorption. The enhancement factor $1 - \mathrm{Re}[\delta D]/D$ has been found in previous work[1,3–5] on the absorption of bulk sound in a 3D electron system. A different result has been obtained in Ref. 2. The reason for this, as discussed in Ref. 4, is the insufficient number of diagrams incorporated in that calculation.

Equation (2) for the scattering cross section can be treated similarly. In the limit $qL \gg 1$, η_{sc} has a dominating forward-scattering component

$$\eta_{sc}(\boldsymbol{q}',\boldsymbol{q}) \sim \delta(\boldsymbol{q}'-\boldsymbol{q}). \tag{42}$$

This property results from the momentum conservation in a translational invariant system.

B. The case $qL \ll 1$

Here, we exploit the diffusion mode representation introduced above. Substituting the density-density correlator, Eq. (25), and the total potential in the strong screening limit, Eq. (36), into Eq. (7) yields

$$\Pi_\omega(\boldsymbol{q},\boldsymbol{q}') = -\nu\frac{(\pi a_B)^2}{A}\sum_{m,n,k,l\geq 1} \times (\beta^{-1})^*_{mn}(\widetilde{G}^{-1})_{nk}(V^{ph}_k)^*(\widetilde{G}^{-1})_{ml}V^{ph}_l. \tag{43}$$

Expanding the bare SAW potential [Eq. (8)] in a series with respect to $|\boldsymbol{qr}| \ll 1$, we find

$$\sum_{l\geq 1}(\widetilde{G}^{-1})_{ml}V^{ph}_l = \frac{1}{\mathcal{L}}\gamma_{\boldsymbol{q}} i q A a_m(\hat{\boldsymbol{q}}), \tag{44}$$

where

$$a_m(\hat{\boldsymbol{q}}) \equiv \sum_{n\geq 1}(\widetilde{G}^{-1})_{mn}\int\frac{d^2\boldsymbol{r}}{A}\hat{\boldsymbol{q}}\boldsymbol{r}\,\psi_n(\boldsymbol{r}). \tag{45}$$

The dimensionless integral in this equation is of order unity for small n's, and it decreases as n increases. $a_m(\hat{\boldsymbol{q}})$ is expected to have the same properties. Introducing result (44) in Eq. (43), we obtain

$$\Pi_\omega(\boldsymbol{q},\boldsymbol{q}') = -\nu(\pi a_B\gamma_{\boldsymbol{q}}q)^2 A\mathcal{L}^{-2} \times \sum_{m,n\geq 1}(\beta^{-1})^*_{mn}a_m(\hat{\boldsymbol{q}})a_n(\hat{\boldsymbol{q}}'). \tag{46}$$

Up to first order in $\delta\beta_{mn}$, the inverse of β_{mn}, Eq. (26), is given by

$$(\beta^{-1})_{mn} = \beta_m^{-1}\delta_{m,n} - \frac{\delta\beta_{mn}}{\beta_m\beta_n} \tag{47}$$

where $\delta\beta_{mn}$ is defined in Eq. (28).

We are now in the position to use Eq. (46) in the evaluation of the absorption and the scattering cross sections. Substituting Eq. (46) into Eq. (1) yields

$$\eta_{abs}(\boldsymbol{q}) = \frac{4\nu}{s\hbar}|\gamma_{\boldsymbol{q}}|^2(\pi a_B)^2 q^2 A^2 \frac{\omega}{D}\sum_{m,n\geq 1}\frac{1}{A\lambda_m} \times\left(\delta_{m,n} - \frac{1}{\lambda_n}\int d^2\boldsymbol{r}\nabla\psi_m(\boldsymbol{r})\nabla\psi_n(\boldsymbol{r}) \times\frac{\mathrm{Re}[\delta D(\boldsymbol{r})]}{D}\right)a_m(\hat{\boldsymbol{q}})a_n(\hat{\boldsymbol{q}}). \tag{48}$$

Note that $A\lambda_m$ is a dimensionless quantity independent of A, cf. Eq. (20). A significant simplification of this equation is achieved when $\delta D(\boldsymbol{r})$ does not vary in space. This is not always the case, of course. We believe, however, that, qualitatively, the influence of the WL effects is described by an average quantity $\delta D=$ const, which will be defined in Sec. VI. Replacing $\delta D(\boldsymbol{r})$ by δD and using the diffusion mode equation (20), Eq. (48) reduces to

$$\eta_{abs}(\boldsymbol{q})=\frac{4\nu}{\hbar}|\gamma_{\boldsymbol{q}}|^2(\pi a_B)^2A^2\frac{q^3}{D}\left(1-\frac{\mathrm{Re}[\delta D]}{D}\right)\times\left\{\sum_{m\geqslant 1}\frac{a_m^2(\hat{\boldsymbol{q}})}{A\lambda_m}\right\}. \tag{49}$$

The dependence on the shape of the dot and the direction of the SAW is comprised in the quantity in braces. The dependences on all other parameters is completely described by its prefactor. As in the case of an infinite system, Eq. (41), the WL corrections enhance the absorption. Comparing Eqs. (41) and (49) we see that η_{abs} is smaller by a factor (q^2A) in the case $qL\ll 1$. That is, a small system absorbs per unit area much less than an extended one. This can be attributed to the fact that the electrons in an extended system can move over the whole period $1/q$ of the piezoelectric field, while a small system restricts this motion by its size.

We evaluate now the scattering cross section. Substituting Eq. (46) into Eq. (2) yields

$$\eta_{sc}(\boldsymbol{q}',\boldsymbol{q})=\frac{q\nu^2}{\pi s^2\hbar^2}|\gamma_{\boldsymbol{q}'}|^2|\gamma_{\boldsymbol{q}}|^2(\pi a_B q)^4A^2\times\sum_{m,n,k,l\geqslant 1}(\beta^{-1})^*_{mn}(\beta^{-1})_{kl}a_m(\hat{\boldsymbol{q}}')a_n(\hat{\boldsymbol{q}})\times a_k(\hat{\boldsymbol{q}}')a_l(\hat{\boldsymbol{q}}). \tag{50}$$

Here, we should replace the matrix elements of β^{-1} by the explicit expressions given in Eq. (47). As far as the WL contributions are concerned, we have to calculate the sum over four a-terms with the $\beta^{-1}\beta^{-1}$ part replaced by

$$-2\ \mathrm{Re}\left[\frac{1}{\beta_m^*}\frac{\delta\beta_{kl}}{\beta_k\beta_l}\right].$$

This can be rewritten as

$$-2\frac{\omega}{D^2\lambda_k\lambda_l}\int d^2\boldsymbol{r}\nabla\psi_k(\boldsymbol{r})\nabla\psi_l(\boldsymbol{r})\left\{\mathrm{Im}[\delta D(\boldsymbol{r})]+\frac{\omega}{D\lambda_m}\mathrm{Re}[\delta D(\boldsymbol{r})]\right\}, \tag{51}$$

showing that the relevant quantity is either $\mathrm{Re}[\delta D(\boldsymbol{r})]$ or $\mathrm{Im}[\delta D(\boldsymbol{r})]$ depending on whether the diffusion time through the dot, A/D, is large or small compared to the period of the SAW.

The replacement of $\delta D(\boldsymbol{r})$ by $\delta D=$ const allows a considerable simplification of expression (51), leading to explicit estimates in the limits of a small and a big dot:

$$\eta_{sc}(\boldsymbol{q}',\boldsymbol{q})\approx\frac{\nu^2}{\pi s^2\hbar^2}|\gamma_{\boldsymbol{q}'}|^2|\gamma_{\boldsymbol{q}}|^2(\pi a_B)^4q^5A^2\times\sum_{m\geqslant 1}a_m(\hat{\boldsymbol{q}}')a_m(\hat{\boldsymbol{q}})\sum_{n\geqslant 1}a_n(\hat{\boldsymbol{q}}')a_n(\hat{\boldsymbol{q}})\times\left\{1-2\frac{\omega}{D\lambda_n}\frac{\mathrm{Im}[\delta D]}{D}\right\}\quad \omega A/D\ll 1$$
$$\times\left(\sum_{m\geqslant 1}\frac{a_m(\hat{\boldsymbol{q}}')a_m(\hat{\boldsymbol{q}})}{A\lambda_m}\right)^2\left(\frac{\omega A}{D}\right)^2\times\left\{1-2\frac{\mathrm{Re}[\delta D]}{D}\right\},\quad \omega A/D\gg 1. \tag{52}$$

The classical contribution and the prefactor of the WL corrections depend strongly on the parameter $A\omega/D$. For a big dot, $A\omega/D>1$, the scattering of SAW's rises faster than A^2 with increasing area A of the dot because the diffusion processes are too slow to screen long wavelength density variations as effectively as short wavelength ones. Indeed, the enhancement factor $\omega A/D$ results from the classical part of $(\beta^{-1})_{mn}$, $\beta_m^{-1}=1-i\omega/D\lambda_m$ [Eq. (28)], which enters Eq. (50) via the inverse of the dielectric matrix. In the small dot case, $\beta_m^{-1}\simeq 1$ for all m starting from unity, and, hence, there is no enhancement factor in the second line of Eq. (52). While the quantum corrections contribute to η_{sc} according to their relative magnitude for big dots, they acquire a small prefactor once $\omega A/D$ becomes smaller than unity. Moreover, since their imaginary part is the relevant quantity in that case, they are small for $\omega<\tau_\phi^{-1}$, cf. Eq. (63) below. This is contrary to the dependence of WL corrections on frequency and phase coherence time as far as the real part of the conductivity is concerned.

VI. WEAK LOCALIZATION CORRECTIONS

The absorption and the scattering cross sections depend on WL corrections via $\delta D(\boldsymbol{r})$, which in turn is directly related to the cooperon $\mathcal{C}_\omega(\boldsymbol{r},\boldsymbol{r})$; see Eq. (23). In the first part of this section, we evaluate the cooperon equation (24). Special attention is devoted to the magnetic field dependence. In the second part, we discuss the approximation of $\delta D(\boldsymbol{r})$ by a spatially independent quantity δD.

A. Magnetic field dependence

In comparison with the diffusion propagator, Eq. (19), the cooperon, Eq. (24), depends on the two additional length scales $l_\phi=\sqrt{D\tau_\phi}$ and $l_B=\sqrt{c\hbar/2eB}$. Due to the sensitivity of quantum corrections to weak magnetic fields, it is sufficient to account perturbatively for the B-dependent terms in Eq. (24). To this end, we expand the cooperon in a power series with respect to $\boldsymbol{A}(\boldsymbol{r})$:

$$\mathcal{C}_\omega(\boldsymbol{r},\boldsymbol{r}')=\mathcal{C}_\omega^{(0)}(\boldsymbol{r},\boldsymbol{r}')+\mathcal{C}_\omega^{(1)}(\boldsymbol{r},\boldsymbol{r}')+\mathcal{C}_\omega^{(2)}(\boldsymbol{r},\boldsymbol{r}')+\cdots, \tag{53}$$

where $\mathcal{C}_\omega^{(m)}\sim\boldsymbol{A}^m$. This expansion can be terminated with a negligible error at the first nonvanishing correction to $\mathcal{C}_\omega^{(0)}(\boldsymbol{r},\boldsymbol{r})$ if $L/l_B\ll 1$ and $|-i\omega+\tau_\phi^{-1}|\gg DL^2/l_B^4$. Using ex-

perimental values (see Sec. VII), we have $\omega \lesssim \tau_\phi^{-1}$, i.e., the second inequality can be written as $L l_\phi / l_B^2 \ll 1$. Since $l_\phi \lesssim L$ in the cases of practical interest, the first condition $L/l_B \ll 1$ determines the range of applicability of the perturbative treatment. Substituting Eq. (53) in Eq. (24) yields

$$
\begin{aligned}
&[-i\omega+\tau_\phi^{-1}-D\nabla^2]\mathcal{C}_\omega^{(0)}(\boldsymbol{r},\boldsymbol{r}')=\delta(\boldsymbol{r}-\boldsymbol{r}'),\\
&[-i\omega+\tau_\phi^{-1}-D\nabla^2]\mathcal{C}_\omega^{(1)}(\boldsymbol{r},\boldsymbol{r}')\\
&\quad=-2iD(2e/c\hbar)\boldsymbol{A}(\boldsymbol{r})\nabla\mathcal{C}_\omega^{(0)}(\boldsymbol{r},\boldsymbol{r}'),\\
&[-i\omega+\tau_\phi^{-1}-D\nabla^2]\mathcal{C}_\omega^{(2)}(\boldsymbol{r},\boldsymbol{r}')\\
&\quad=-2iD(2e/c\hbar)\boldsymbol{A}(\boldsymbol{r})\nabla\mathcal{C}_\omega^{(1)}(\boldsymbol{r},\boldsymbol{r}')\\
&\qquad-D[(2e/c\hbar)\boldsymbol{A}(\boldsymbol{r})]^2\mathcal{C}_\omega^{(0)}(\boldsymbol{r},\boldsymbol{r}'),
\end{aligned}
\tag{54}
$$

where we have used the gauge $\nabla \boldsymbol{A}(\boldsymbol{r})=0$. The boundary conditions are given by

$$
\begin{aligned}
&\nabla_n\mathcal{C}_\omega^{(0)}|_b=0,\\
&\nabla_n\mathcal{C}_\omega^{(m+1)}|_b=i(2e/c\hbar)\boldsymbol{A}_n\mathcal{C}_\omega^{(m)}|_b, \quad \text{for } m=0,1,\ldots.
\end{aligned}
\tag{55}
$$

The equation for $\mathcal{C}_\omega^{(0)}$ can be solved using the diffusion modes defined in Eq. (20)

$$
\mathcal{C}_\omega^{(0)}(\boldsymbol{r},\boldsymbol{r}')=\sum_{m=0}^{\lambda_m\lesssim l^{-2}}\frac{\psi_m(\boldsymbol{r})\psi_m(\boldsymbol{r}')}{-i\omega+D\lambda_m+\tau_\phi^{-1}}. \tag{56}
$$

There is a cut-off on the summation because the diffusion approximation is valid on scales larger than the mean free path. The relevant frequency scale is given by $|-i\omega+\tau_\phi^{-1}|\approx\tau_\phi^{-1}$.

Since $\mathcal{C}_\omega^{(0)}$ is the Green's function for the differential operator of all three equations (54), it enables us to write down solutions for $\mathcal{C}_\omega^{(1)}$ and $\mathcal{C}_\omega^{(2)}$ as well. The result for $\mathcal{C}_\omega^{(1)}$ reads

$$
\begin{aligned}
\mathcal{C}_\omega^{(1)}(\boldsymbol{r},\boldsymbol{r}')=D&\oint d\boldsymbol{S}_1[i(2e/c\hbar)\boldsymbol{A}_n(\boldsymbol{r}_1)\mathcal{C}_\omega^{(0)}(\boldsymbol{r}_1,\boldsymbol{r}')]\mathcal{C}_\omega^{(0)}(\boldsymbol{r}_1,\boldsymbol{r})\\
&+\int d^2\boldsymbol{r}_1[-2iD(2e/c\hbar)\boldsymbol{A}(\boldsymbol{r}_1)\nabla_1\mathcal{C}_\omega^{(0)}(\boldsymbol{r}_1,\boldsymbol{r}')]\\
&\times\mathcal{C}_\omega^{(0)}(\boldsymbol{r}_1,\boldsymbol{r}).
\end{aligned}
\tag{57}
$$

The first term represents an integral over the boundary of the dot and includes the inhomogeneity of the boundary condition (55), whereas the second one accounts for the source term in the differential equation. Rewriting the surface integral in terms of a volume integral shows that $\mathcal{C}_\omega^{(1)}(\boldsymbol{r},\boldsymbol{r})=0$, i.e., the quantum corrections do not depend linearly on the magnetic field. The expression for $\mathcal{C}_\omega^{(2)}$ has the same structure as Eq. (57), one has just to substitute the corresponding source terms given in Eqs. (54). That is,

$$
\begin{aligned}
\mathcal{C}_\omega^{(2)}(\boldsymbol{r},\boldsymbol{r}')=D&\oint d\boldsymbol{S}_1[i(2e/c\hbar)\boldsymbol{A}_n(\boldsymbol{r}_1)\mathcal{C}_\omega^{(1)}(\boldsymbol{r}_1,\boldsymbol{r}')]\mathcal{C}_\omega^{(0)}(\boldsymbol{r}_1,\boldsymbol{r})\\
&+\int d^2\boldsymbol{r}_1\{-2iD(2e/c\hbar)\boldsymbol{A}(\boldsymbol{r}_1)\nabla_1\mathcal{C}_\omega^{(1)}(\boldsymbol{r}_1,\boldsymbol{r}')\\
&-D[(2e/c\hbar)\boldsymbol{A}(\boldsymbol{r}_1)]^2\mathcal{C}_\omega^{(0)}(\boldsymbol{r}_1,\boldsymbol{r}')\}\mathcal{C}_\omega^{(0)}(\boldsymbol{r}_1,\boldsymbol{r}).
\end{aligned}
\tag{58}
$$

This equation and Eq. (56) determine the WL correction to the diffusion coefficient in the form $\delta D(\boldsymbol{r})=-(D/\pi\hbar\nu)[\mathcal{C}_\omega^{(0)}(\boldsymbol{r},\boldsymbol{r})+\mathcal{C}_\omega^{(2)}(\boldsymbol{r},\boldsymbol{r})]$. Since $\mathcal{C}_\omega^{(2)}\sim B^2$, the physical quantities calculated in the preceding section are invariant with respect to a reversal of the direction of the magnetic field.

B. The average quantity δD

The spatially constant quantity δD that was used in Sec. V is introduced by

$$
\delta D(\boldsymbol{r})\to\delta D\equiv-\frac{D}{\pi\hbar\nu A}\int d^2\boldsymbol{r}\mathcal{C}_\omega(\boldsymbol{r},\boldsymbol{r}). \tag{59}
$$

This approximation captures the essential features of the problem and becomes exact in two limiting cases. For small frequencies and large phase coherence times, $|-i\omega+\tau_\phi^{-1}|\ll D/A$, the cooperon is determined by the zeroth diffusion mode ψ_0, and hence $\mathcal{C}_\omega(\boldsymbol{r},\boldsymbol{r})\approx$const. In the opposite case, the bulklike diffusion process guarantees that at least $\mathcal{C}_\omega^{(0)}(\boldsymbol{r},\boldsymbol{r})$ is spatially uniform except near the boundaries. In the intermediate regime, $|-i\omega+\tau_\phi^{-1}|\simeq D/A$, we expect a smooth cross-over between these two limiting cases.

In the limiting cases one is able to obtain explicit results for the averaged WL correction δD. Depending on whether $A|-i\omega+\tau_\phi^{-1}|/D$ is smaller or larger than unity, it is convenient to replace the zero-field cooperon $\mathcal{C}_\omega^{(0)}$ in the solution for $\mathcal{C}_\omega^{(2)}$ Eq. (58), by its diffusion mode representation (56) or its Fourier representation for an infinite 2D system,

$$
\mathcal{C}_\omega^{(0)}(\boldsymbol{r},\boldsymbol{r}')=\int\frac{d^2\boldsymbol{q}}{(2\pi)^2}\frac{e^{i\boldsymbol{q}\cdot(\boldsymbol{r}-\boldsymbol{r}')}}{-i\omega+Dq^2+\tau_\phi^{-1}}, \tag{60}
$$

respectively. In the former case, we are able to separate the large contributions due to the zero mode from the corrections resulting from all other modes. In the latter, the particle diffuses on scales small compared to the size of the system; hence, the boundary conditions imposed on a finite dot can be disregarded.

1. Small dot case

Substituting Eq. (56) in $\mathcal{C}_\omega^{(2)}$, Eq. (58), yields

$$
\begin{aligned}
\int d^2\boldsymbol{r}\mathcal{C}_\omega(\boldsymbol{r},\boldsymbol{r})=\sum_{m=0}^{\lambda_m\lesssim l^{-2}}\Bigg[&-i\omega+D\lambda_m+\tau_\phi^{-1}\\
&+D\int d^2\boldsymbol{r}\psi_m^2(\boldsymbol{r})[(2e/c\hbar)\boldsymbol{A}(\boldsymbol{r})]^2\\
&+D^2\sum_{n=0}^{\lambda_n\lesssim l^{-2}}\frac{(F_{nm}-F_{mn})^2}{-i\omega+D\lambda_n+\tau_\phi^{-1}}\Bigg]^{-1},
\end{aligned}
\tag{61}
$$

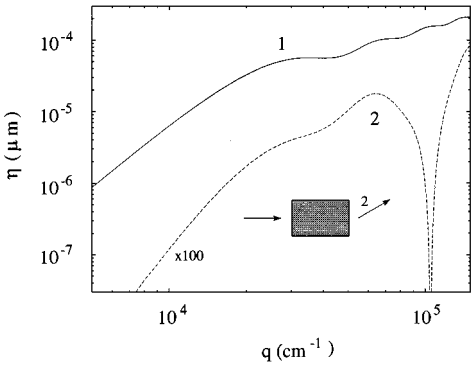

FIG. 3. Double logarithmic plot of the absorption and the scattering cross sections as a function of the wave vector.

where

$$F_{mn}=\int d^2\boldsymbol{r}\psi_m(\boldsymbol{r})i(2e/c\hbar)\boldsymbol{A}(\boldsymbol{r})\nabla\psi_n(\boldsymbol{r}). \tag{62}$$

For $A|-i\omega+\tau_\phi^{-1}|/D<1$, we restrict the sum to the $m=0$ term and obtain

$$\delta D=-\frac{D}{\pi\hbar\nu A}\frac{1}{-i\omega+\tau_\phi^{-1}+c_1DA/l_B^4}, \tag{63}$$

where c_1 is a real positive constant of order unity. The lowest eigenmode ψ_0 leads to an increase of the WL corrections as the area A of the dot decreases. This behavior results from the fact that the boundaries of an isolated system cause no phase breaking. In the case where the dot is connected to leads, the summation over modes starts at $m=1$ and yields[21] $\delta D=-(\pi\hbar\nu)^{-1}\ln(A/l^2)$ for $B=0$. That is, the correction term decreases as the dot shrinks, since the effective phase coherence length is determined by the separation of the contacts. The scales of the critical magnetic field at which the phase coherence is significantly reduced are different for isolated and open systems as well. This field can be deduced from Eq. (61) by equating the two field dependent terms

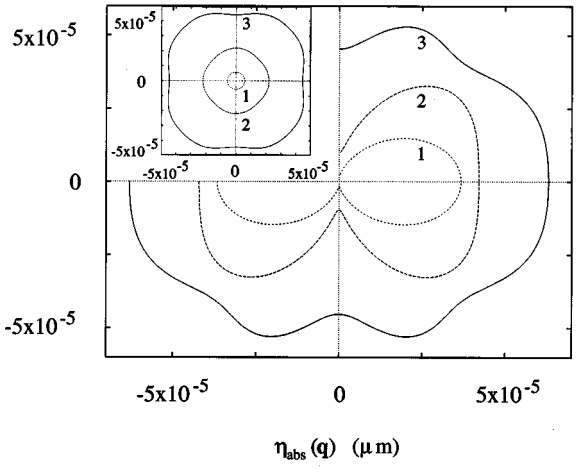

FIG. 4. Polar diagrams of the absorption cross section of a rectangular (main plot) and a square dot (inset) as a function of the angle of incidence of the SAW. Results for three different wave numbers q are given.

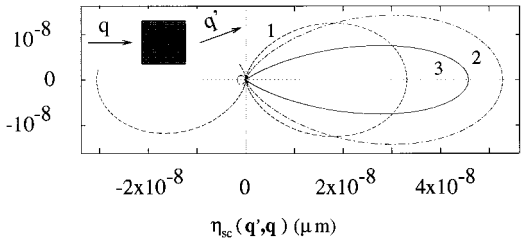

FIG. 5. Polar diagram of the elastic scattering cross section of a square dot as a function of the direction $\boldsymbol{q}'$ of the outgoing wave. The angle of incidence ($\boldsymbol{q}$) is kept fixed; see inset.

(which are of the same order) to the first one. For an isolated dot, the first term is of order $|-i\omega+\tau_\phi^{-1}|$, Eq. (63), whereas it is given by D/A for a dot coupled to leads. This results in the estimates

$$(l_B^4)^{iso}\simeq A\min\{D/\omega,l_\phi^2\},\quad (l_B^4)^{lead}\simeq A^2. \tag{64}$$

The critical field for an isolated small dot is thus much larger than for a dot with leads.

2. Big dot case

For $A|-i\omega+\tau_\phi^{-1}|/D>1$, we substitute Eq. (60) in $\mathcal{C}_\omega^{(2)}$, Eq. (58), and obtain

$$\delta D=\frac{c_2}{\pi\hbar\nu}\ln\{\tau[-i\omega+\tau_\phi^{-1}+c_3DA/l_B^4]\}, \tag{65}$$

where c_2 and c_3 are real positive constants of order unity. In this case, the zeroth mode plays no role; Eq. (65) is valid independently of the boundary conditions imposed.

We note that the characterization as ''big'' or ''small'' dot does not necessarily apply simultaneously to both the diffusion propagator [Eq. (19)] and the cooperon [Eq. (56)]. In particular, for $\omega\tau_\phi\ll1$, there exists the situation where the diffusion propagator [responsible for the classical contributions] is determined by the zeroth mode since $A\omega/D\ll1$, whereas the cooperon [determining δD] behaves bulklike since $A\tau_\phi^{-1}/D\gg1$.

VII. NUMERICAL CALCULATIONS

To compute numerically the scattering and the absorption cross sections, we have used an accurate inversion of the dielectric function $\epsilon(\boldsymbol{r},\boldsymbol{r}')$; see Eq. (33). This procedure covers small and large values of the parameter qL. Thus, the numerical results bridge the gap left by the analytical study of limiting cases in Sec. V, and provide information about the angular dependence of the cross sections. The scaling of the numerically calculated cross sections with respect to A,q,D, etc. can be used to confirm the predictions derived analytically, cf. Eqs. (41)–(52). In Figs. 3–5 discussed below, results for different wave vectors q are shown; all other parameters are kept fixed. This means that the two dimensionless quantities qL and $A\omega/D$ vary. Since the latter, even for the largest wave vectors used is smaller than unity, it is essentially the effects of the variation of qL which we focus on. In this small dot case, the WL corrections are essentially described by the quantity $1-\mathrm{Re}[\delta D]/D$, cf. Eqs. (49) and (52), which is discussed in connection with Fig. 6.

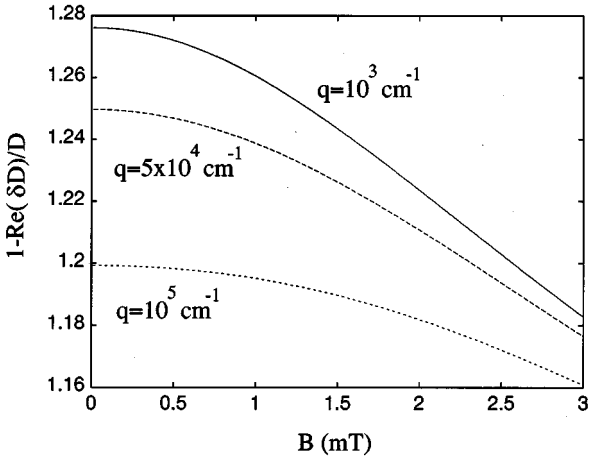

FIG. 6. Weak localization enhancement $1-\mathrm{Re}[\delta D]/D$, Eq. (59), of the absorption cross section, Eq. (49), as a function of the magnetic field B for three different wave numbers.

The dot has the shape of a square (lengths $L_x=L_y$) or a rectangle ($L_x>L_y$). In the first case emphasis is put on the angular dependence associated with the value of qL. We use the following values for the physical quantities which apply to GaAs/Al_xGa_{1-x}As heterostructures: $\nu=1.55\times10^{10}$ $\mathrm{meV}^{-1}\mathrm{cm}^{-2}$, $s=2.7\times10^5$ $\mathrm{cm\,s}^{-1}$, $D=140$ $\mathrm{cm}^2\,\mathrm{s}^{-1}$ ($l=0.1$ μm), $\tau=0.4$ ps, $\tau_\phi=0.03$ ns, $d=0.1$ μm, $a_B=10.6$ nm, $\epsilon_0=12.8$, $\epsilon_1=1$, and, e.g., $L_x=L_y=0.66$ μm for the square dot. The phase coherence time (corresponding to $T=0.1$ K and $l_\phi=0.63$ μm) and the diffusion coefficient for a low mobility electron gas are taken from Ref. 22. The choice of a small diffusion coefficient is dictated by the condition that the size of the dot is larger than the mean free path, but small enough to allow for $qL<1$ and $qL>1$ in the range of reasonable sound frequencies. For these frequencies and the quantities given above, ω and τ_ϕ^{-1} are smaller than D/A. Thus, the diffusion propagator [Eq. (19)] and the cooperon [Eq. (56)] are essentially determined by the zeroth mode. Since the very existence of the zeroth mode relies on the assumption of an isolated dot, it is this physical regime that puts the most emphasis on the noninvasive character of the proposed SAW measurement. Posing the requirement $q<l^{-1}$ yields $q\approx10^5$ cm^{-1} ($\omega\approx2\pi\times4.3$ GHz) as the upper limit for the applicability of the diffusion approximation. A lower limit $\omega>\Delta$ could arise from the finiteness of the mean level spacing $\Delta=(\nu A)^{-1}$ in the quantum dot. For $A\simeq1$ $\mu\mathrm{m}^2$, we have $\Delta\simeq6$ μeV corresponding to $\omega\simeq10^{10}$ s^{-1}. We argue, however, that inelastic level broadening smears out the discreteness of the one-particle levels, rendering the spacing Δ irrelevant. Indeed, using the phase coherence time introduced above, we find $\hbar/\tau_\phi\simeq20$ $\mu\mathrm{eV}>\Delta$. That is, a lower limit for the frequency is not required.

Figure 3 shows in a double-logarithmic plot the absorption and the scattering cross sections for a rectangular dot ($L_x=1.7$ μm, $L_y=1$ μm) as a function of the wave vector $\boldsymbol{q}\|x$. Here and in Figs. 4 and 5 the term $\hat{q}_x\hat{q}_y$ of the electron-surface phonon vertex, Eq. (9), has been replaced by its maximum $\frac{1}{2}$; its angular dependence is not taken into account because it depends on the orientation of the dot with respect to the lattice axes. Quantum corrections for $B=0$ are incorporated. The absorption cross section is given by curve 1. The part to the left of label 1 exhibits the behavior $\eta_{abs}\sim q^3$, confirming the power law predicted by Eq. (49) for the limit $qL\ll1$. The remaining part of the curve corresponds to $\eta_{abs}\sim q$. This behavior is anticipated in the regime $qL\gg1$; see Eq. (41). The oscillations of $\eta_{abs}(\boldsymbol{q})$ represent geometric resonances. Maxima appear around $qL_x=2\pi m$, $m=1,2,\ldots$, whereas minima occur for $qL_x=\pi(2m+1)$. The curve labeled 2 (corresponding to the direction 2) represents results for the scattering cross section for a scattering angle of 30°. It follows the power law $\eta_{sc}\sim q^5$, Eq. (52), in the limit $qL\ll1$. For $qL\gg1$, the scattering cross-section behaves in a sample and angle specific way. In this case, the magnitude of $\eta_{sc}(\boldsymbol{q}'\neq\boldsymbol{q})$ is small compared to the forward-scattering component, which continues to grow as q^5; cf. Eq. (42) and Fig. 5.

Figure 4 shows results for the absorption cross section of a rectangular ($L_x=1.2$ μm, $L_y=0.4$ μm; main plot) and a square dot ($L_x=L_y=0.66$ μm; inset). The abscissa of the figure agrees with the x axis of the dot. Figure 4 represents a polar diagram for $\eta_{abs}(\boldsymbol{q})$, i.e., the distance of a data point from the origin corresponds to the magnitude of η_{abs}, whereas the orientation of the wave vector $\boldsymbol{q}$ of the SAW agrees with the direction of the line joining the data point and the origin. The curves labeled 1, 2, and 3 correspond to the wave vectors $q_1=10^4$ cm^{-1}, $q_2=5\times10^4$ cm^{-1}, and $q_3=10^5$ cm^{-1}, respectively. The magnitude of the curves labeled 1 is increased by a factor of 20. The main plot in Fig. 4 for the rectangular dot shows a strong anisotropy of the absorption cross section for the two smaller wave vectors. For instance, η_{abs} for $\boldsymbol{q}_1\|x$ and η_{abs} for $\boldsymbol{q}_1\|y$ deviate by a factor of about 20 from each other. This pronounced anisotropy can be attributed to the fact that the relevant size of the dot (either L_x or L_y) enters Eq. (49) for η_{abs} as a high power in the limit $qL<1$. In contrast, for the largest wave vector q_3, η_{abs} exhibits only a minor dependence on the angle of incidence, reflecting that only the total area is relevant in the regime $qL\gg1$; cf. Eq. (40). That is, for an approximate isotropy of η_{abs} to appear, both qL_x and qL_y have to be sufficiently larger than unity. As can be seen from the inset of Fig. 4, the situation is somewhat different in the case of a square dot. Here, η_{abs} is completely independent of the direction of incidence for the smallest wave vector q_1. The absorption cross section acquires a weak angular dependence with increasing wave vector, which can be attributed to geometrical resonances occurring for $qL\geqslant2\pi$.

The curves presented in Fig. 4 include WL corrections for zero magnetic field, which increase the absorption. This enhancement is given by the factor $1-\mathrm{Re}[\delta D]/D$ independent of q for the ''small-dot'' case; cf. Eqs. (49) and (63). Indeed, all numerical calculations indicated that the curves with and without quantum corrections exhibit practically the same angular dependence, merely the magnitudes differ by a constant factor. We discuss the enhancement factor $1-\mathrm{Re}[\delta D]/D$ separately below.

Figure 5 presents results for the elastic scattering cross section of a square dot. A polar representation is chosen with respect to the direction of the outgoing phonon $\hat{\boldsymbol{q}}'$. The direction of incidence $\hat{\boldsymbol{q}}$ is shown in the inset. The labels 1, 2,

and 3 of the curves indicate the wave vectors used, $q_3=2q_2=10q_1=10^5$ cm^{-1}. Because of the significant dependence of η_{sc} on the magnitude of q, the data of curve 1 are multiplied by 10^3, while that of curve 3 are divided by 15 and those of curve 2 are not changed. Generally, the scattering cross section of the square dot shows a weak dependence on the angle of incidence but varies considerably with the scattering angle θ, i.e., $\theta=\sphericalangle(\hat{\boldsymbol{q}}',\hat{\boldsymbol{q}})$. In particular, the angular dependence of η_{sc} in the regime $qL<1$ (curve 1) is given by $\eta_{sc}\sim\cos^2\theta=(\hat{\boldsymbol{q}}\hat{\boldsymbol{q}}')^2$. With increasing wave number q, the $\cos^2\theta$ law is gradually replaced by an enhancement of forward scattering and a suppression of back scattering (Mie effect, cf. Ref. 23, p. 654.). For $q=q_2$, only a small backscattering component is left. For even larger q, e.g., $q=q_3$, this component is not resolved on the scale of Fig. 5. This confirms Eq. (42). In agreement with our qualitative analysis, quantum corrections are extremely small for the parameters introduced above. The curves in Fig. 5 correspond therefore essentially to the classical part of the scattering cross-section.

In the small dot case, the WL corrections to the absorption cross section are significant, whereas the scattering cross section remains practically unaffected. To illustrate the dependence of the WL corrections on the magnetic field, the frequency and the temperature, we have evaluated $1-\mathrm{Re}[\delta D]/D$ for the cooperon expression (61). For the small dot, we expect δD to be determined by the lowest mode. According to Eq. (63),

$$-\delta D/D=\Delta\tau_\phi/\pi\hbar=0.23, \tag{66}$$

where we have used $\omega<\tau_\phi^{-1}$ and $B=0$. The right-hand side follows from the numerical values listed above. In Fig. 6, $1-\mathrm{Re}[\delta D]/D$ is shown as a function of the magnetic field for a square dot ($L_x=L_y=0.66$ μm). The deviations of the numerical results from the estimate (66) arise from the contributions of the higher modes. The assumption $l_B>L$ used in Sec. V is valid for $B<1.4$ mT. The continuation of the curves to stronger magnetic fields can only serve as an indication for the further suppression of the WL corrections with increasing B. The three curves in Fig. 6 show how the enhancement factor decreases with increasing frequency. Assuming[22] $\tau_\phi\sim T^{-1}$, the increase of the temperature from $T=0.1$ K to $T=1$ K corresponds to a reduction of the phase coherence length from $l_\phi=0.63$ μm (which is used in Fig. 6) to $l_\phi=0.2$ μm. The latter value is significantly smaller than the size of the dot, $L=0.66$ μm, leading to $1-\mathrm{Re}[\delta D]/D\approx1.07$ for $B=0$. The relative differences between the three curves shown in Fig. 6 become much smaller as well.

VIII. DISCUSSION

We have calculated the absorption and the scattering cross sections of a SAW for an isolated quantum dot. The dependence of these quantities on WL corrections has been found. In addition, we have calculated the WL corrections to the attenuation coefficient Γ_q of an extended 2DEG [Eq. (41)]. Since these corrections can (at least) approximately be expressed in terms of the spatial average of the change of the diffusion coefficient, they are given in a similar way as those to the conductivity. One can therefore use results derived in that case to establish the dependence of the cross sections and Γ_q on spin-orbit scattering, scattering by magnetic impurities, etc.[19] We emphasize the WL corrections because they are expected to play a significant role in the experimental investigation of the effects discussed in this paper. Indeed, though the classical cross sections depend strongly on A and ω, these parameters are fixed once the dot and interdigital transducers are defined on a sample. But it is relatively easy to vary the temperature and the magnetic field, which both affect only the WL corrections. Note also that the SAW technique allows precise measurements of the relative changes of the transmitted wave intensity, whereas the absolute attenuation is much less easily detectable. That is, it is more difficult to resolve the large but constant classical effects than the quantum corrections, which can be ''tuned'' by external parameters. The measurement of the absorption cross section (or Γ_q) as a function of the temperature directly yields the dependence of the phase coherence time on T. For typical values, $\omega\tau_\phi<1$, and, hence, it is the parameter A/l_ϕ^2 that determines whether the dot has to be considered as a small or big one. Thus, the temperature can also shift the dot from one regime to another.

One may also consider an array of quantum dots. Since the electron-phonon coupling is weak (even for the piezoelectric interaction), it is reasonable to assume that the response of a dot array to a SAW can be represented by a superposition of the effects associated with isolated dots. To underscore this point, let us give some numerical estimates for the SAW attenuation and the electron heating. To estimate whether the calculated cross sections are within the experimental sensitivity, we convert the absorption cross section to an attenuation coefficient by $\Gamma_q\simeq\eta_{abs}/A$; cf. Eq. (40). This amounts to densely covering the area between the transducers with quantum dots. Using $\eta_{abs}\simeq10^{-4}$ μm and $A\simeq1$ μm^2 yields an attenuation of about 10 dB/cm. The relative change of the attenuation due to WL effects is then about 1 dB/cm. This value is about ten times larger than the highest resolution achieved, suggesting that the signal of a much less dense arrangement of dots can be measured.

To estimate the effect of electron heating, one has to compare the temperature of the dot with $\Delta T\equiv I\eta_{abs}\tau_\epsilon/k_B$, where I is the flux intensity of the incoming surface wave and τ_ϵ is the energy relaxation time. Using $w\approx2$ mm for the length and the width of a macroscopic SAW delay line and $P\approx1$ μW for the total SAW intensity,[13] we determine $I=P/w$. The energy relaxation time τ_ϵ can roughly be identified with the phase coherence time τ_ϕ. (This is a good estimate in the case where both τ_ϵ and τ_ϕ result from electron-electron scattering.[19]) Using the values $\tau_\phi=30$ ps and $\eta_{abs}\simeq10^{-4}$ μm, we obtain $\Delta T\simeq0.1$ K, which represents a significant change in the temperature range of interest.

ACKNOWLEDGMENTS

Financial support by the German-Israeli Foundation, the Fund for Basic Research of the Israel Academy of Sciences and Humanities, and the Deutsche Forschungsgemeinschaft (A. K.) is gratefully acknowledged. We thank Y. Galperin, A. Kamenev, D. Khmelnitzkii, D. Klakow, C. Rocke, M. Rotter, A. Tilke, and A. Wixforth for valuable discussions.

[1] A. Houghton and H. Won, J. Phys. C **18**, 2507 (1985).
[2] B. G. Kotliar and T. V. Ramakrishnan, Phys. Rev. B **31**, 8188 (1985).
[3] V. V. Afonin, Y. M. Galperin, and R. N. Ignat'ev, Fiz. Tverd. Tela (Leningrad) **28**, 1063 (1986) [Sov. Phys. Solid State **28**, 594 (1986)].
[4] T. R. Kirkpatrick and D. Belitz, Phys. Rev. B **34**, 2168 (1986).
[5] M. Y. Reizer, Phys. Rev. B **40**, 7461 (1989).
[6] R. A. Serota, Phys. Rev. B **38**, 12 640 (1988).
[7] S. Hershfield and M. Y. Reizer, Phys. Rev. B **43**, 9475 (1991).
[8] G. W. Farnell, in *Acoustic Surface Waves*, edited by A. A. Oliner (Springer, Berlin, 1978).
[9] A. Mayer, Phys. Rep. **256**, 237 (1995).
[10] V. W. Rampton, K. McEnaney, A. G. Kozorezov, P. J. A. Carter, C. D. W. Wilkinson, M. Henin, and O. H. Hughe, Semicond. Sci. Technol. **7**, 641 (1992).
[11] A. Wixforth, J. P. Kotthaus, and G. Weimann, Phys. Rev. Lett. **56**, 2104 (1986).
[12] A. Wixforth, J. Scriba, M. Wassermeier, J. P. Kotthaus, G. Weimann, and W. Schlapp, Phys. Rev. B **40**, 7874 (1989).
[13] A. Schenstrom, Y. J. Qian, M. F. Xu, H. P. Baum, M. Levy, and B. K. Sarma, Solid State Commun. **65**, 739 (1988).
[14] R. L. Willett, M. A. Paalanen, R. R. Ruel, K. W. West, L. N. Pfeiffer, and D. J. Bishop, Phys. Rev. Lett. **65**, 112 (1990).
[15] F. Guillion, A. Sachrajda, M. D'Iorio, R. Boulet, and P. Coleridge, Can. J. Phys. **69**, 461 (1991).
[16] J. M. Shilton, D. R. Mace, V. I. Talyanskii, Y. Galperin, M. Y. Simmons, M. Pepper, and D. A. Ritchie, J. Phys. Condens. Matter **8**, L337 (1996).
[17] A. Knäbchen, Y. B. Levinson, and O. Entin-Wohlman, Phys. Rev. B **54**, 10 696 (1996).
[18] S. H. Simon (unpublished).
[19] B. L. Altshuler and A. G. Aronov, in *Electron-Electron Interaction in Disordered Systems*, edited by A. L. Efros and M. Pollak (North-Holland, Oxford, 1985).
[20] D. Vollhardt and P. Wölfle, Phys. Rev. B **22**, 4666 (1980).
[21] E. Abrahams, P. W. Anderson, D. C. Licciardello, and T. V. Ramakrishnan, Phys. Rev. B **42**, 673 (1979).
[22] C. W. J. Beenakker and H. van Houten, in *Quantum Transport in Semiconductor Nanostructures*, Vol. 44 of *Solid State Physics*, edited by H. E. Ehrenreich and D. T. Turnbull (Academic Press, Boston, 1991).
[23] M. Born and E. Wolf, *Principles of Optics* (Pergamon, Oxford, 1975).